RESEARCH PAPER

Superior Photocatalytic Efficiency with Titania (TiO_2)-Polyaniline (PANI) Nanocomposite for Rapid Carbol Fuchsin (CF) Dye Degradation

Satish Arvind Ahire[1], Ashwini Ashok Bachhav[2], Bapu Sonu Jagdale[3], Thansing Bhavsing Pawar[3], Prashant Bhimrao Koli[4], Dnyaneshwar Suryabhan Sanap[5], Arun Vitthal Patil[6,*]

* *aruptl@gmail.com*

[1] Department of Chemistry, Maharaja Sayajirao Gaikwad Arts, Science and Commerce College, Malegaon, Nashik (Affiliated to Savitribai Phule Pune University, Pune (MH), India)
[2] MVPs College of Pharmacy, Nashik. (Affiliated to Savitribai Phule Pune University, Pune (MH), India)
[3] Department of Chemistry, Loknete Vyankatrao Hiray Arts, Science and Commerce College, Panchavati, Nashik. (Affiliated to Savitribai Phule Pune University, Pune (MH)
[4] Department of Chemistry, Karmaveer Abasaheb, N.M. Sonawane Arts Commerce and Science College, Satana, Taluka-Baglan, District- Nashik. (Affiliated to Savitribai Phule Pune University, Pune (MH), India)
[5] Department of Chemistry, KPG Arts, Commerce, and Science College Igatpuri-422402, Savitribai Phule Pune University, Pune, Maharashtra, India
[6] Department of Physics, Arts, Science and Commerce College, Surgana, Nashik. (Affiliated to Savitribai Phule Pune University, Pune (MH), India)

Received: January 2024 **Revised: May 2024** **Accepted: May 2024**
DOI: 10.22068/ijmse.3511

Abstract: *Hybrid photocatalysts, comprising both inorganic and organic polymeric components are the most promising photocatalysts for the degradation of organic contaminants. The nanocomposite, Titania-Polyaniline (TiO_2-PANI) was synthesized using the chemical oxidative polymerization method. Various characterization techniques were employed to assess the properties of the catalysts. The ultraviolet diffuse reflectance spectroscopy (UV-DRS) analysis revealed that the TiO_2 absorbs only UV light while the TiO_2-PANI nanocomposite absorbs light from both UV and visible regions. The X-ray diffraction (XRD) results confirmed the presence of TiO_2 (anatase) in both TiO_2 nanoparticles and TiO_2-PANI (Titania-Polyaniline) nanocomposite. The phases of the catalysts were verified through Raman, TEM, and SAED techniques where all results are in good agreement with each other. The average crystallite size of TiO_2 nanoparticle and TiO_2-PANI nanocomposite were 13.87 and 10.76 nm. The thermal stability of the catalysts was assessed by the Thermal gravimetric analysis (TGA) technique. The order of the thermal stability is TiO_2 >TiO_2-PANI >PANI. The crystal lattice characteristics were confirmed using Transmission electron microscopy (TEM). The surface area measurements were confirmed from the Brunauer-Emmett-Teller (BET) study and were employed for the evaluation of the photocatalytic efficiency of both, TiO_2 nanoparticles and TiO_2-PANI nanocomposite catalysts. The energy dispersive spectroscopy (EDS) study was employed for elemental detection of the fabricated materials. Raman spectroscopy was employed for the chemical structure and the phase characteristics of the materials. The standard conditions for the degradation of the CF dye were 8 g/L of catalyst dosage, 20 mg/L of dye concentration, and a pH of 7. The TiO_2-PANI nanocomposite exhibited superior efficiency as compared to pure TiO_2 nanoparticles, achieving almost 100% degradation in just 40 minutes.*

Keywords: *TiO_2–PANI nanocomposite, Carbol fuchsin dye, TEM, Water purification, Scavenging study.*

Graphical Abstract:

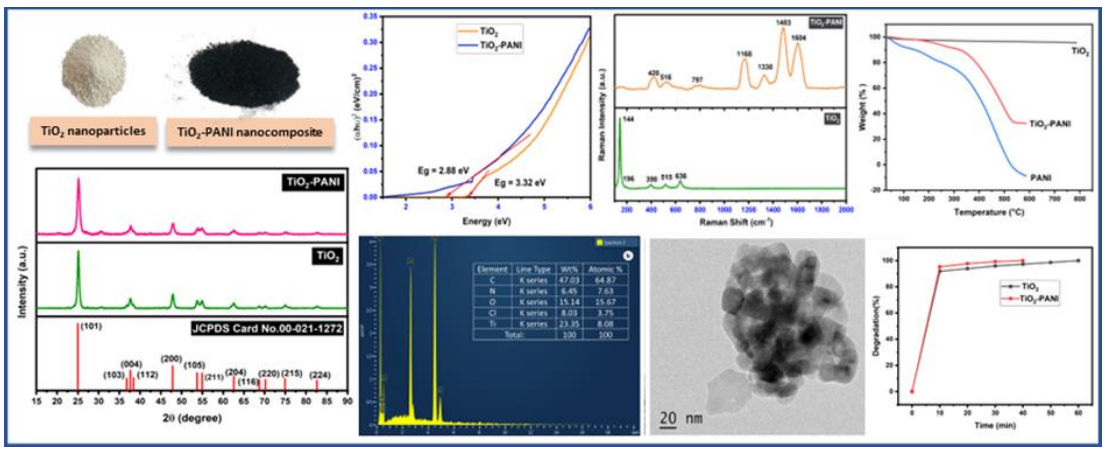

[DOI: 10.22068/ijmse.3511]

1. INTRODUCTION

One of the greatest challenges facing humans and other life forms on earth is pollution, which refers the contamination of physical and biological constituents of the earth or atmosphere [1, 2]. Environmental pollution comprises any human activity that deteriorates the quality of the natural environment and is characterized as air, water, and soil pollution [3–5]. Water pollution is particularly alarming due to its essential role in sustaining life [6]. The primary contributor to water pollution includes discharge from dyes, pharmaceutical, cosmetics, fertilizer, and pesticide industries [3, 7, 8]. Among these, the dye industry stands out as a significant source of environmental degradation as various dyes are extensively used in sectors like food, cosmetics, textiles, and pharmaceutical sectors, resulting in global production of 1000000 tonnes worldwide [9]. According to the World Bank Report, approximately 17 to 20% of water pollution can be attributed to the dyeing and processing of textiles [10]. Many studies revealed that a substantial portion (20%) of pollution occurs during the synthesis and processing operations of the textile industry, leading to wastewater discharge [11, 12]. These discharged dyes contain numerous chemicals, each with toxic levels, posing threats to aquatic life and humans. Most dyes are water-soluble, non-biodegradable compounds with carcinogenic properties, adversely impacting water quality and increasing the BOD (biochemical oxygen demand) and COD (chemical oxygen demand) [13, 14]. In recent times, the challenge of eliminating dyes and other pollutants from the environment has become a focal point for researchers. Consequently, various methods including biological treatment [15], catalytic reduction [16], adsorption [17], and photocatalytic degradation [18, 19] have been employed to address this environmental concern. Among these approaches, photocatalytic degradation has gained significant popularity for effectively removing pollutants, surpassing traditional methods [10, 20].

The photocatalytic properties of the inorganic semiconductor have garnered significant attention due to its band gap energy of 3 to 3.2 eV, non-toxicity, high chemical and photostability, cost-effectiveness and versatile applications [21–23]. At standard pressure, TiO_2 exists in various crystalline forms, including anatase, rutile, and brookite [24, 25], each exhibiting distinct physical properties such as refractive index and chemical and photochemical activity [26]. Among these phases, anatase shows greater photocatalytic activity than rutile TiO_2 for pure phases [27]. Photocatalysis using TiO_2 is an advanced oxidation process that uses reactive oxygen species to oxidize almost all organic contaminants without creating any toxic by-products [22, 28, 29]. The photocatalytic efficiency of the TiO_2 is greatly influenced by crystallographic structure, morphology, and particle size [30].

Surface modification methods extensively utilize conducting polymers due to their ease of synthesis, high conductivity and stability, and excellent environmental capability. These polymers such as polythiophene, polypyrrole, and polyaniline (PANI), enhance photocatalytic performance by extending photo response to visible light [31, 32]. Polyaniline (PANI) in particular, stands out as a common conducting polymer with unique electrical, optical, and photoelectric characteristics, making it cost-effective compared to other conducting polymers [33–35]. Notably, PANI is typically considered as a p-type semiconductor, while TiO_2 is an n-type semiconductor, forming a p-n junction heterostructures when combined [36]. This combination results in a hybrid nanocomposite with enhanced flexibility, improved processability, exceptional transparency, good conductivity, and stability [33, 36]. By mitigating the rate of the electron-hole pair recombination, the hybrid nanocomposite not only augments the stability of the catalyst but also enhances its photocatalytic activity [10]. Numerous studies in the literature underscore the superior effectiveness of hybrid nanocomposites compared to their bare counterparts [37–43].

This study's noteworthy findings and contributions to existing work emphasize that polymer-based nanocomposites, such as TiO_2-PANi, present a more favorable option than simple transition metal-doped or multidoped metal oxide nanocomposite materials. Notably, the TiO_2/PANI matrix exhibits high efficiency in reducing organic contaminants like CF dye. This approach holds promise for future research in fabricating novel polymer-based catalysts for organic decontamination as part of effluent

[DOI: 10.22068/ijmse.3511]

treatment.

2. EXPERIMENTAL PROCEDURES

2.1. Materials

The chemicals employed in this research were all of the AR grade and were utilized without additional purification. In the synthesis of TiO_2, Titanium (IV) isopropoxide (TIP) and anhydrous ethanol were employed while in the synthesis of TiO_2-PANI nanocomposite Aniline, Ammonium persulphate (APS), and hydrochloric acid (HCl, 1 M) were utilized.

The TiO_2 nanomaterial was synthesized using the sol-gel method [44, 45]. Initially, a solution containing titanium (IV) isopropoxide (TIP) (10 ml) and anhydrous ethanol underwent 30 minutes of sonication. Subsequently, deionized water (20 mL) was added dropwise to the sonicated mixture. Following complete water addition, the mixture was stirred continuously for 24 hours, resulting in the formation of a white-coloured precipitate. This precipitate was then separated, subjected to washing with deionized water, dried, and ultimately subjected to calcination in a muffle furnace at 500ºC for 3 hours.

The TiO_2-PANI nanocomposite was synthesized at room temperature through the chemical oxidative method [46]. Initially, a mixture comprising TiO_2 (1 g), aniline (1 mL), and 1 M HCl was taken in a beaker labelled as 'A'. Subsequently, this solution underwent 30 minutes of sonication in an ultrasonic bath. After sonication, another solution of Ammonium persulphate (APS) (2.5 g) in 1 M HCl was prepared in a separate beaker labelled as 'B'. The solution from beaker 'B' was added gradually to the beaker 'A' and the resulting mixture was agitated overnight. Following 24 hours, a precipitate formed, which was then filtered, washed with deionized water and acetone, and finally dried at 80°C for 1 hour.

2.2. Characterizations

The synthesized materials namely, TiO_2 and TiO_2/PANI nanocomposite underwent comprehensive characterization employing advanced techniques including UV analysis were performed using Shimadzu UV 2450 spectrophotometer. X-Ray Diffraction Spectrosocpy (XRD) pattern of the material was measured by a Bruker D8 Advance diffractometer. Raman spectra were measured on Renishaw InVia Raman microscope equipped with a 532 nm laser. The SEM and EDS analysis was performed using Jeol 6390LA/OXFORD XMX N. The TEM and SAED pattern was achieved using Jeol/JEM 2100 Model.

2.2.1. Ultraviolet Diffuse reflectance spectroscopy (UV-DRS)

This technique is commonly employed for determining the optical properties and band gap energy of materials. It is a simple, rapid, and cost-effective method [47]. The UV analysis of the samples was conducted using a UV double-beam spectrophotometer.

3. RESULTS AND DISCUSSION

In Figure 1 the absorbance spectra of both TiO_2 nanoparticle and TiO_2-PANI nanocomposite are illustrated. The results indicate that TiO_2 nanoparticles absorb light from the UV region. The total solar energy accounts for 3% of the UV light. This limited light absorption directly influences the generation of the electron-hole pair, consequently, diminishing the photocatalytic efficiency of the TiO_2.

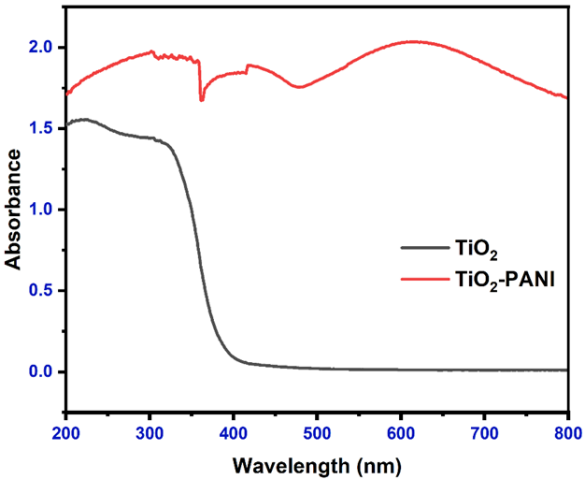

Fig. 1. Absorbance Spectra of the bare TiO_2 and TiO_2-PANI nanocomposite

In contrast, TiO_2-PANI nanocomposite exhibits light absorption across both UV and visible regions, encompassing a significant portion of the solar spectrum. This higher light absorption results in an augmented generation of electron-hole pairs, thereby enhancing the photocatalytic performance of TiO_2-PANI nanocomposite. Moreover, PANI possesses an extended π

[DOI: 10.22068/ijmse.3511]

electron system, contributing to increased charge separation and additional catalyst features [48–52]. The calculation of band gap energy(Eg) was performed by the method proposed by Tauc in 1966 [53]. According to this method, the absorption coefficient (α) is defined by Equation 1.

$$(\alpha h\nu)^{1/\gamma} = B\,(h\nu - E_g) \quad (1)$$

Where h= Planck constant, ν= photon frequency, E_g= the band gap energy and B= the constant. The γ depends on the type of electronic transition. For the direct band gap and indirect transition band gap, this factor is equivalent to ½ or 2 respectively [54]. The band gap energy of both materials was calculated using Equation 1. The Tauc plot used for the calculation of Eg is shown in Figure 2 whereas Table 1 shows the calculated band gap energy of both TiO_2 nanoparticles and TiO_2-PANI nanocomposites.

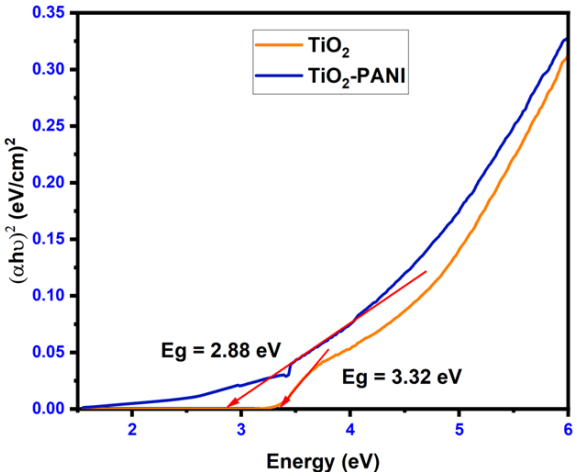

Fig. 2. Tauc plot for the TiO_2 nanoparticles and TiO_2-PANI nanocomposite

3.1.1. X-ray diffraction (XRD) study

The XRD technique provides information on the crystal structure, crystallite size, and strain [58]. The resulting pattern, depicted in Figure 3. The pattern was obtained using CuKα$_1$ radiations and a monochromator with a wavelength (λ= 1.54060 Å) at 25°C. The catalysts were analyzed from Bragg's angle ranging from 10-90°. The TiO_2 exhibited 2θ values at 25.15, 36.78, 37.64, 38.40, 47.82, 53.72, 54.94, 62.61, 68.71, 70.18, 74.94, and 82.58° corresponding to (101), (103), (004), (112), (200), (105), (211), (204), (116), (220), (215) and (224) crystal planes of the anatase TiO_2, characterized by a tetragonal phase and space group I41/amd. The XRD spectra were consistent with the JCPDS card no. 00-021-1272 [59]. The anatase phase of the TiO_2, especially with its (101) plane, as illustrated60, as depicted in Figure 4. The XRD results of both TiO_2 nanoparticles and the TiO_2-PANI nanocomposite confirm the formation of the crystalline tetragonal anatase phase of TiO_2. The peak XRD peak of PANI was observed at 15.40, 20.56, 25.38 and 32.77° and these peaks are in good agreement with the peaks reported in the literature [61, 62].

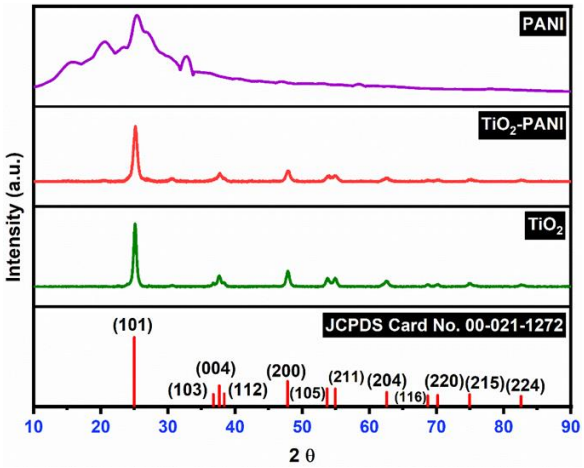

Fig. 3. XRD spectrum of the bare TiO_2 and TiO_2-PANI nanocomposite

In the XRD of TiO_2-PANI nanocomposite, a broad suppressed diffraction peak of PANI was observed at 20.50°, indicative of its amorphous nature [49, 63, 64]. The peak position in the modified TiO_2-PANI nanocomposite exhibited a slight shift and broadening compared to the TiO_2 peak position. This observation implies that the presence of PANI has a limited impact on the crystal structure. The average crystallite size for both TiO_2 nanoparticles and TiO_2-PANI nanocomposite was determined using Equation 2. i.e. the Scherrer equation [65].

$$D = \frac{K.\lambda}{\beta_{1/2}\cos\theta} \quad (2)$$

Table 1. Band gap energies of the TiO_2 nanoparticles and TiO_2-PANI nanocomposites

Name of the Catalyst	Calculated(eV)	Reported(eV)	Reference
TiO_2	3.32	3.2	[55, 56]
TiO_2-PANI	2.88	2.97	[57]

[DOI: 10.22068/ijmse.3511]

where D= average crystallite size of the material, K= Scherrer constant (0.89), λ= wavelength of the X-ray used, $\beta_{1/2}$= full width at half maximum (FWHM) of the diffracted peak, θ= diffraction angle.

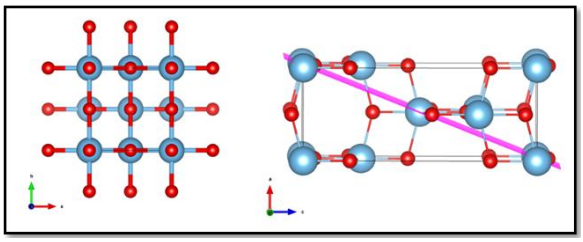

Fig. 4. Crystal structure of Anatase TiO_2 and its (101) plane

Table 2 presents average crystallite size for both TiO_2 nanoparticles and TiO_2-PANI nanocomposite. The TiO_2-PANI nanocomposite exhibited a decreased average crystallite size, attributed to interfacial interactions and the attachment of PANI on the surface of the TiO_2 [63].

Table 2. The average crystallite size of the prepared material

Material	Average Crystallite Size (nm)
TiO_2	13.87
TiO_2-PANI	10.76

3.1.2. Scanning electron microscopy (SEM) study

The SEM technique plays a crucial role in assessing the surface topography of various materials [66, 67]. In this study, SEM analysis of the sample was conducted using the Jeol 6390LA/ OXFORD XMX Nanocomposite instrument. Figure 5(a) displays the SEM images of TiO_2, revealing a porous structure. Notably, the TiO_2 nanoparticles exhibit agglomeration due to the high surface energy, leading to a reduction in the effective surface area and a subsequent decrease in photocatalytic activity. Conversely, Figure 5(b). Illustrates the modified TiO_2 in a more separated state. This observed separation is attributed to the presence of PANI on the surface, which hinders the agglomeration process by creating repulsive forces between particles, thereby preventing their agglomeration [33]. Numerous studies have highlighted that the addition of PANI enhances the photocatalytic efficiency of TiO_2-PANI nanocomposite [33, 68–71].

3.1.3. Energy Dispersive Spectroscopy (EDS or EDAX)

This technique offers insights into the elemental composition of the material, providing both qualitative and quantitative information [65, 72]. The EDAX was conducted using Jeol 6390LA/ OXFORD XMX Nanocomposite instrument. Figure 6 displays the EDAX of TiO_2 nanoparticles, revealing the presence of Ti (32.99%) and (O) (67.01%).

In contrast, the EDAX of TiO_2-PANI, depicted in Figure 7, indicates the presence of Ti (8%), (O) (15.67%), C (64.87%), N (7.63%) and Cl (8.08%) elements. The detection of traces of Cl can be attributed to the hydrochloric acid during the synthesis of the nanocomposite [49].

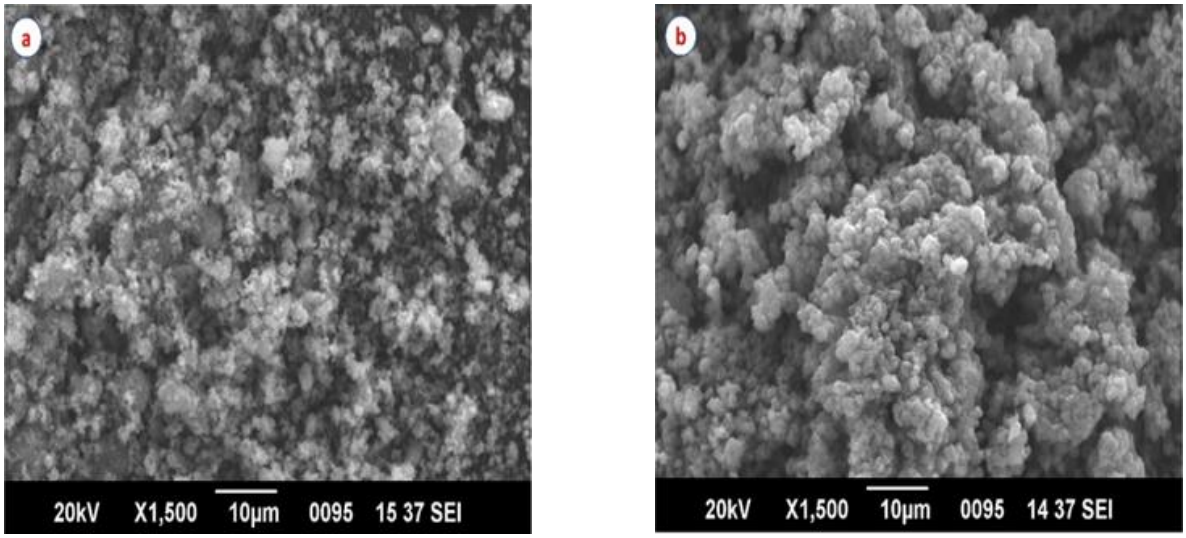

Fig. 5. SEM images for (a) TiO_2 nanoparticles and (b) TiO_2-PANI nanocomposite

[DOI: 10.22068/ijmse.3511]

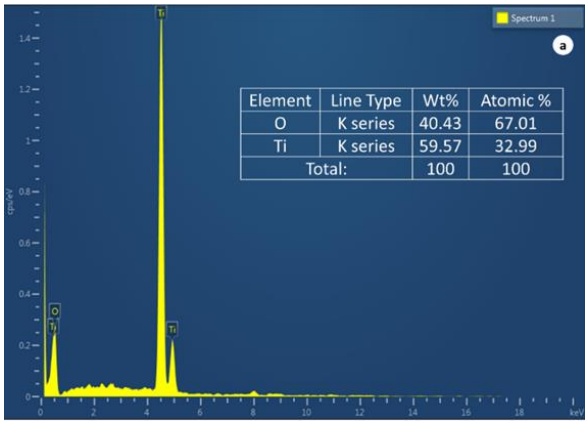

Fig. 6. EDAX spectrum of TiO_2

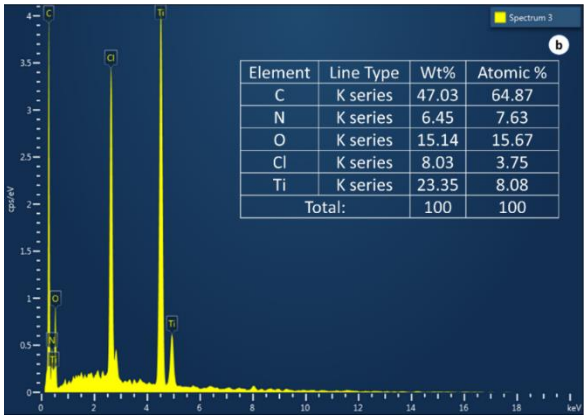

Fig. 7. EDAX spectrum of the TiO_2-PANI nanocomposite

3.1.4. *Raman spectroscopy*

The Raman technique serves as a valuable tool for obtaining insights into the chemical structure and the phase characteristics of the materials [73, 74]. Figure 8 illustrates the Raman spectrum of both TiO_2 nanoparticles and TiO_2-PANI nanocomposite.

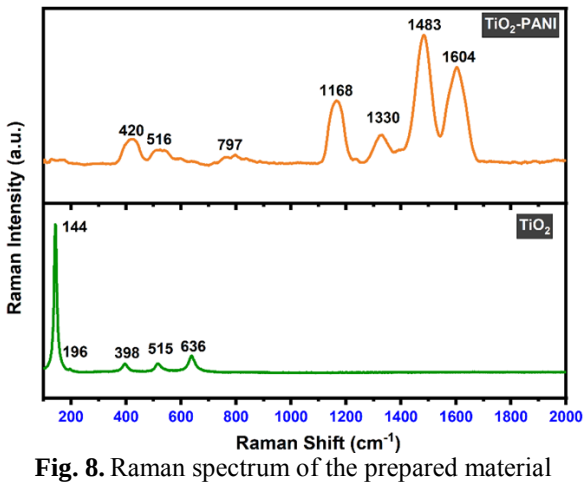

Fig. 8. Raman spectrum of the prepared material

The Raman spectrum of TiO_2 shows five prominent peaks at 144 (Eg), 196 (Eg), 398 (B1g), 515 (A1g) and 636 cm^{-1} (Eg). The results of both XRD and Raman spectra are in good agreement, suggesting the existence of the anatase phase of TiO_2 [75]. On the other hand, the Raman spectrum of the TiO_2-PANI nanocomposite indicates shifts in the bands at 398 and 515 cm^{-1} of TiO_2, to 420 and 516 cm^{-1} respectively. Additionally, the band at 144 cm^{-1} is suppressed due to the presence of PANI [76]. The PANI-specific bands were observed at 797 cm^{-1} (C-H distortion), 1168 cm^{-1} (C-H bending vibration of the quinoid and benzenoid rings), 1330 cm^{-1} (stretching vibrations of C-C of the quinoid ring), 1483 cm^{-1} (the N-H stretching) and 1604 cm^{-1} (stretching vibrations of C-C of the benzenoid) [76–78].

3.1.5. *Thermogravimetric analysis (TGA)*

This method proves valuable in assessing the thermal stability of a substance of the substance [79]. Figure 9 presents the TGA of PANI, TiO_2 nanomaterial, and TiO_2-PANI nanocomposite. The TGA of TiO_2 exhibits a minor weight loss attributed to the release of adsorbed water during its synthesis [80]. Notably, the TGA results indicate that TiO_2 demonstrates higher thermal stability compared to the other substances. On the other hand, the TGA curve of PANI reveals three distinct weight losses. The initial loss, occurring at 20 to 140°C, is attributed to water loss. The second weight loss, observed from 150 to 320°C, results from the loss of dopant acid and water of crystallization. The third weight loss, occurring at 350 to 520°C, is associated with the degradation of PANI [68].

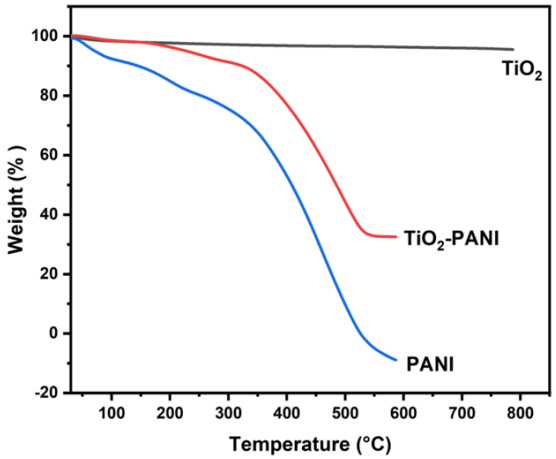

Fig. 9. TGA of PANI, TiO_2, and TiO_2-PANI nanocomposite

[DOI: 10.22068/ijmse.3511]

The TGA curve of TiO_2/PANI shows two distinct weight losses. The initial weight loss, occurring from 50 to 200°C, is due to water loss. The subsequent weight loss, at 300 to 540°C, is associated with the degradation of the low molecular weight oligomer of PANI. Remarkably, no weight loss of the nanocomposite is observed beyond 550°C, emphasizing the stability of the TiO_2, nanoparticles. These findings confirm the formation of the TiO_2/PANI nanocomposite [68]. The thermal hierarchy of the fabricated material, as depicted in Figure 9**,** is established as TiO_2 >TiO_2-PANI >PANI.

3.1.6. High resolution-Transmission electron microscopy (HR-TEM) study

The TEM technique reveals the surface morphology of the material, offering high-resolution images [81]. The TEM analysis of the sample was conducted using the Jeol JEM 2100 instruments, with Figure 10 displaying the TEM images of the TiO_2-PANI nanocomposite. The images depict the TiO_2 nanoparticles embedded within the polymer chain, resulting in noticeable agglomeration [31, 46, 82].

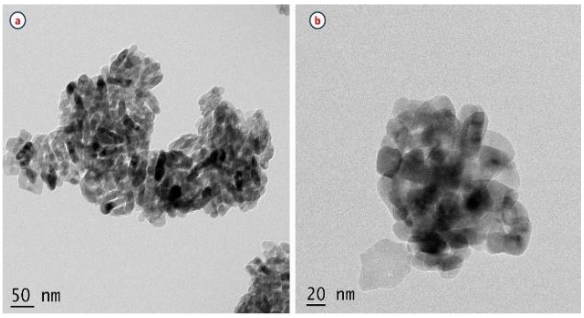

Fig. 10. TEM of TiO_2-PANI nanocomposite

Figure 11 exhibits various lattice planes with a lattice spacing of 0.33 nm, distributed in diverse directions. This lattice spacing functions as confirmation of the presence anatase phase of the TiO_2 nanoparticles [81].

Figure 12, the selected area electron diffraction (SAED) pattern of TiO_2-PANI nanocomposite is presented. The diffraction ring pattern in SAED of TiO_2-PANI nanocomposite validates the presence of the polycrystalline anatase TiO_2 [83, 84]. The lattice planes identified in SAED are in good agreement with those predicted by the XRD technique.

The Brunauer-Emmett-Teller (BET) study was investigated for fabricated materials, namely TiO_2 and TiO_2/PANI nanocomposite. The N_2 adsorption and desorption experiment was employed to generate the BET adsorption isotherm.

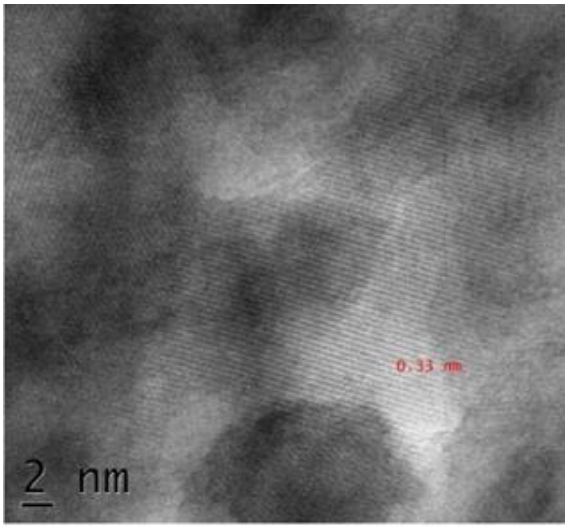

Fig. 11. Lattice spacing in TiO_2-PANI nanocomposite

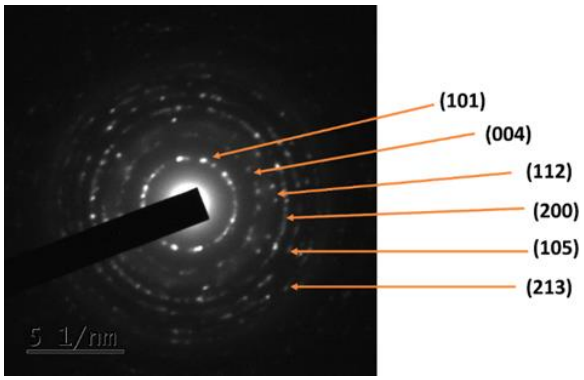

Fig. 12. SAED pattern of the TiO_2-PANI nanocomposite

3.1.7. Brunauer-Emmett-Teller (BET) study

The BET graph was constructed using the parameters of relative pressure (P/P_0) against total gas adsorbed under standard temperature and pressure conditions on the catalyst's surface. The investigation of surface area is a crucial parameter for any catalyst, facilitating effective surface interaction between chemical entities. Figure 13 illustrates the BET figures for both materials. From BET investigation provided essential surface parameters, including total surface area, pore size/volume, and correlation coefficient for both the fabricated materials, as detailed in Table 3.

The bare TiO_2 exhibited a total BET surface area

[DOI: 10.22068/ijmse.3511]

and pore radius of 53.7433 m^2/g and 80.12 A°, respectively. In comparison, the TiO_2/PANI nanocomposite displayed a BET surface area and pore radius of 51.4774 m^2/g and 78.56, respectively. The slight reduction in surface area for the modified TiO_2 is due to the embedding of TiO_2 nanoparticles in the polymer chain, leading to agglomeration. The BET investigation revealed that the BET curves for both materials, TiO_2 and TiO_2/PANI nanocomposite, correspond to type V adsorption isotherm, one of the six types in the BDDT system of adsorption isotherms. The type V is indicative of porous materials.

3.2. Photocatalytic Study

The assessment of photocatalytic efficiency for both TiO_2 nanoparticles and TiO_2-PANI nanocomposite was conducted using the Carbol fuchsin dye. All experiments were carried out in a reactor with a Hg vapor lamp as the light source. Batch experiments were performed, varying catalyst doses of 2, 4, 6, and 8 g/L, and dye concentrations of 20, 40, 60, and 80 mg/L. Each batch solution was exposed to the light and at 10-minute intervals, samples were withdrawn, followed by centrifugation. Subsequently, the absorbance of the solution was measured and recorded after each run. This process was iterated till a constant or zero absorbance was achieved. The degradation efficiency of the catalyst was calculated using Equation 3:

$$\text{Degradation (\%)} = \left(\frac{C_o - C_t}{C_o}\right) \times 100 \quad (3)$$

Where C_o = concentration of Carbol fuchsin before irradiation (t= 0) and C_t= concentration at time t after given irradiation.

3.2.1. *Parameters Optimization*

The photocatalytic investigation was conducted at λ_{max}= 550 nm. The optimal conditions for the degradation of Carbol Fuchsin were 8 g/L catalyst dosage, a 20 mg/L dye concentration, and a pH= 7. Further details and discussions on the results are presented in section 3.2.2 onwards.

3.2.2. *Effect of catalyst dose*

This parameter was explored by variation in the catalyst dosage within the range from 2 g/L to 8 g/L. In the same experiment, a constant dye concentration of 40 mg/L was employed across all series of batch experiments. The degradation efficiency of both TiO_2 nanoparticles and TiO_2-PANI nanocomposite was calculated using Equation 3 and the results are shown in Figure 14. Remarkably, the percent degradation exhibited an increase, due to an increase in catalyst dosage.

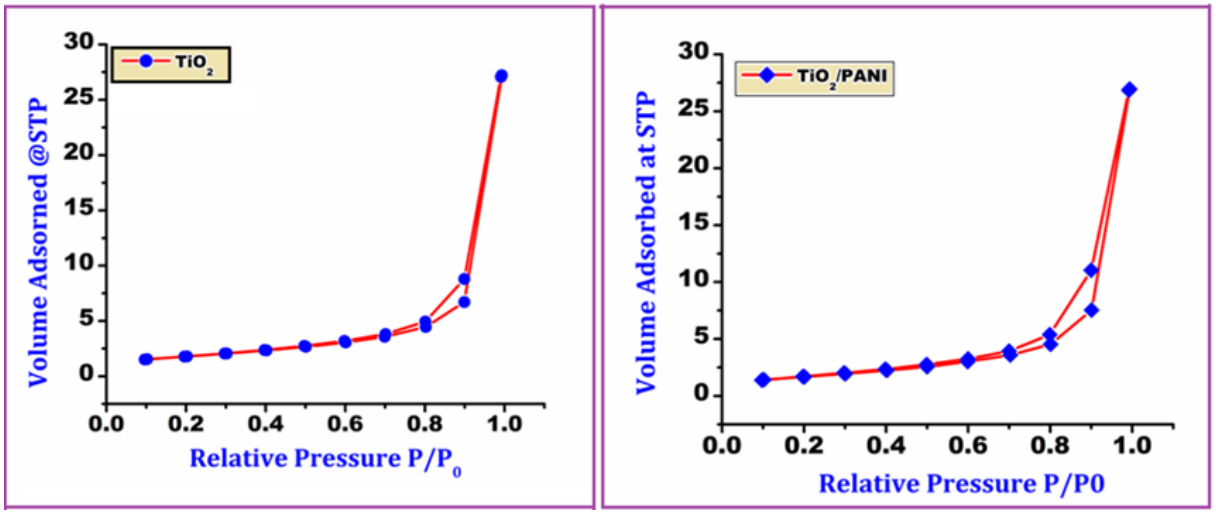

Fig. 13. Brunauer-Emmett-Teller nitrogen adsorption-desorption spectrum for bare TiO_2 and TiO_2/PANI nanocomposite material

Table 3. The BET characteristics of pore volume, surface area, and pore diameter for TiO_2 and TiO_2/PANI nanocomposite

Fabricated Material	Surface Area (m^2/g)	Pore volume (cc/g)	Pore radius (Å)	Correlation Coefficient (R^2)
TiO_2	53.7433	0.159	80.12	0.9999
TiO_2/PANI	51.4774	0.160	78.56	0.9999

[DOI: 10.22068/ijmse.3511]

This escalation in degradation is the consequence of the increase in the number of active sites of the catalyst, crucial for efficient photocatalysis [85]. Consequently, the optimal degradation was attained at a catalyst dose of 8 g/L for both TiO_2 nanoparticles and TiO_2-PANI nanocomposite.

It is essential to note that TiO_2 predominantly absorbs UV light, constituting only 3% of total solar energy. This limitation hampers the generation of electron-hole pairs. Thereby reducing the degradation rate. Additionally, TiO_2 possesses a small band gap of about 2.88 eV, leading to rapid recombination of electron-hole pair, further limiting its photocatalytic efficiency. The incorporation of PANI overcomes these drawbacks and enhances the photocatalytic properties of the TiO_2-PANI nanocomposite.

PANI exhibits a high absorption coefficient for visible light, a significant portion of solar energy, and effectively delays the electron-hole recombination process. Consequently, photocatalytic efficiency gets enhanced and the TiO_2-PANI nanocomposite emerges as an exceptional catalyst for the CF dye degradation, surpassing the performance of TiO_2 nanoparticles.

3.2.3. *Effect of initial dye concentration*

This is a significant step in exploring the photocatalytic performance of the material. In this experiment, we investigated the impact of varying dye concentrations, especially at 20, 40, 60, and 80 mg/L. The catalyst dose was kept fixed at 8 g/L for each set of experiments. The degradation efficiency of TiO_2 nanoparticles and TiO_2-PANI nanocomposite was determined using Equation 3 and the results are shown graphically in Figure 15.

Analysis of the results, revealed a decline in the percentage degradation as the dye concentration increased. The reduction in degradation can be attributed to the accumulation of the dye molecules on the catalyst surface, leading to an increase in path length for light penetrating the solution. Furthermore, this accumulation obstructs the catalyst's surface, diminishing light absorption and impeding the generation of the electron-hole pairs. Consequently, an increase in dye concentration correlates with a decrease in the photocatalytic efficiency of the catalyst. This study concluded that optimal degradation was attained at lower dye concentrations[85]. The observed trend was consistent for both for both TiO_2 and TiO_2-PANI nanocomposites. Remarkably, TiO_2-PANI nanocomposite exhibited superior efficiency compared to TiO_2., achieving 96.05 % degradation.

3.2.4. *pH optimization*

The catalytic processes of a catalyst are significantly influenced by the pH since the catalyst's surface is pH-dependent. Understanding the point of zero charge (PZC) is crucial in gaining insights into the catalyst surface. Consequently, experiments were conducted to ascertain the PZC of TiO_2 nanoparticles. The recorded pH change is graphically depicted in Figure 16**,** revealing the PZC value 7 for the TiO_2 catalyst [86]. A comparative study of photocatalytic efficiency of both, TiO_2 and TiO_2-PANI nanocomposite was carried out at pH 7, as the PZC value for pure TiO_2 is obtained as 7. (as mentioned in the PZC experiment).

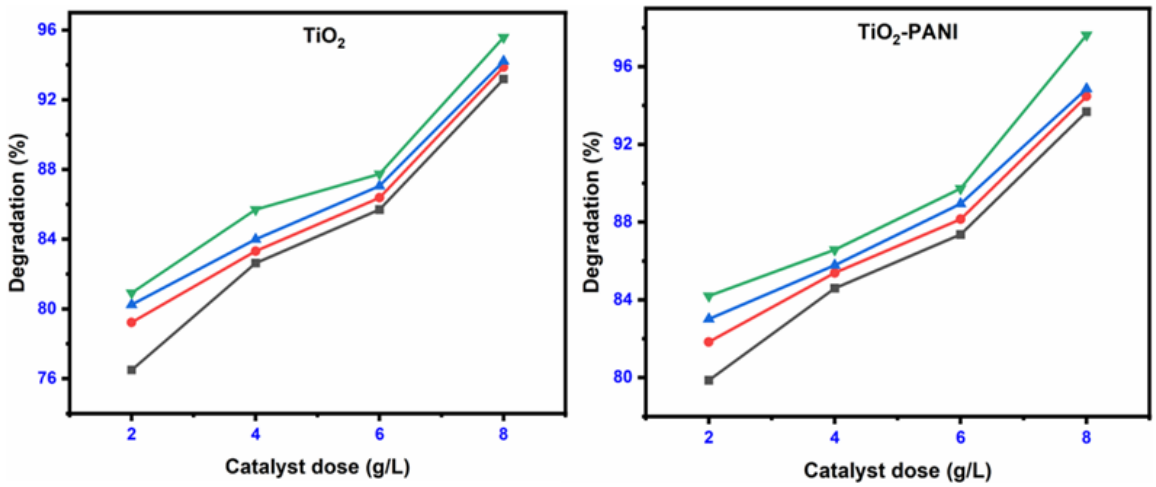

Fig. 14. Effect of catalyst dose of TiO_2 nanoparticle and TiO_2-PANI nanocomposite on the rate of degradation of CF

[DOI: 10.22068/ijmse.3511]

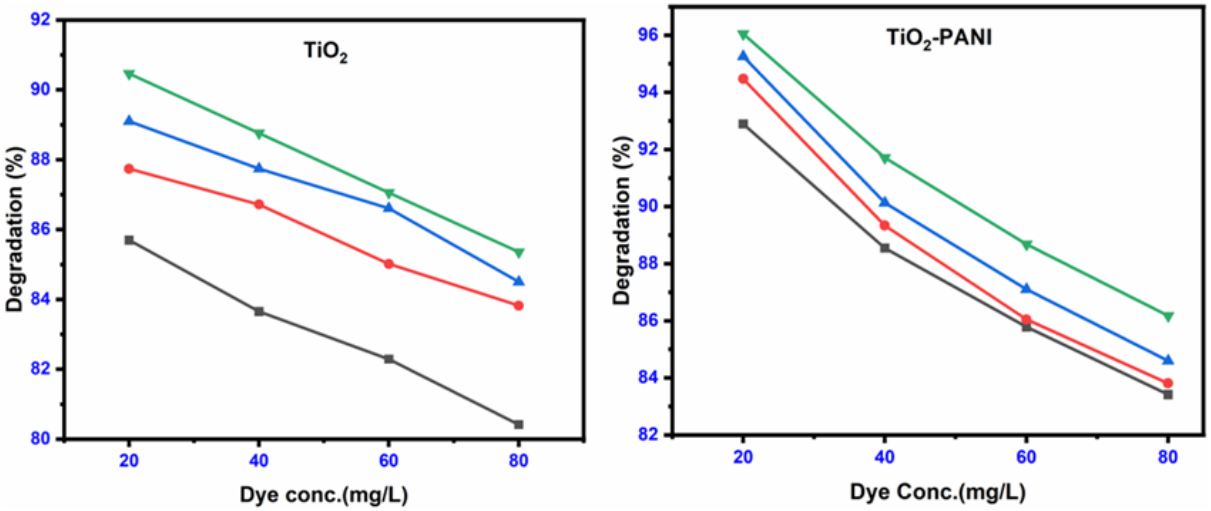

Fig. 15. Effect of Initial dye concentration on the rate of degradation using TiO_2 nanoparticle and TiO_2-PANI nanocomposite

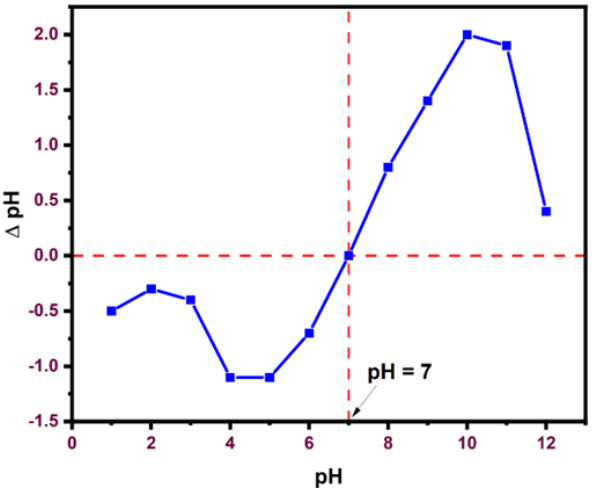

Fig. 16. Point of Zero Charge (PZC) of TiO_2

The pH range selected for further 5 to 8. Batch experiments were executed with a consistent catalyst dose of 8 g/L and dye concentrations set at 20 mg/L. The pH was varied for each batch. The results show an increase in the degradation rate up to pH 7, followed by a subsequent decrease as depicted in Figure 17). The maximum degradation, reaching about 100%, was observed at pH 7 for TiO_2 nanoparticles. Hence, pH 7 was chosen for a comparative assessment of the photocatalytic performance of the TiO_2-PANI nanocomposite.

3.2.5. Effect of contact time

Initially, a catalyst dose of 8 g/L and a CF dye concentration of 20 mg/L were taken into a beaker. The solution's pH was maintained at a constant value of 7. Subsequently, the solution was placed in a photo reactor and the absorbance measurements were conducted at 10 minute intervals. The same experimental procedure was executed for both, TiO_2 nanoparticles and TiO_2-PANI nanocomposites.

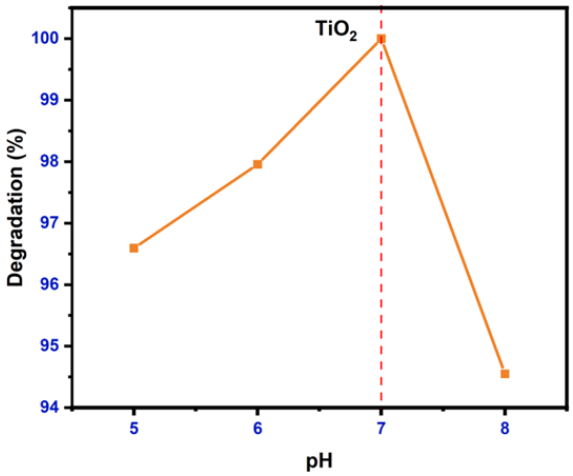

Fig. 17. Effect of pH on degradation of the CF dye using TiO_2 nanoparticles.

The degradation efficiency of both TiO_2 nanoparticles and TiO_2-PANI nanocomposite was determined using Equation 3 and the outcomes are presented in Figure 18.

The findings from this study revealed that the TiO_2 achieved almost 100% of the within 60 minutes. On the other hand, the TiO_2-PANI nanocomposite exhibited almost 100% of CF dye degradation in just 40 minutes. This experiment proves that the TiO_2-PANI nanocomposite was the most efficient catalyst than TiO_2

[DOI: 10.22068/ijmse.3511]

nanoparticles. The degradation efficiency of the TiO_2-PANI nanocomposite was due to the addition of PANI, which enhances light absorption in both UV and visible regions and inhibits electron-hole recombinations [87].

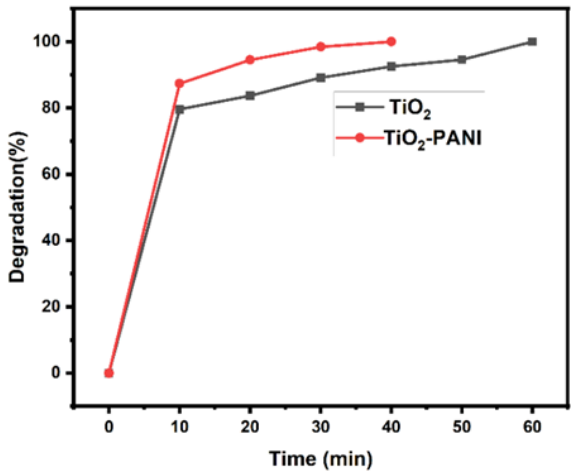

Fig. 18. Effect of Contact Time on Degradation of CF dye

Figure 19 displays the mass spectrums of the both raw dye and the treated dye solution. In Figure 19 (a), the presence of a peak at 330.20 is associated with the actual molecular weight of the dye, contributing to its coloration. When this is compared with the mass spectrum of the treated dye solution in Figure 19 (b), the intensity of the peak at 330.20 is notably reduced. This reduction becomes even more apparent in Figure 19 (c), signifying the cleavage of bonds within the dye. Consequently, the base peak at 223.14 and other fragment peaks emerge. These outcomes confirm the complete degradation of the CF dye.

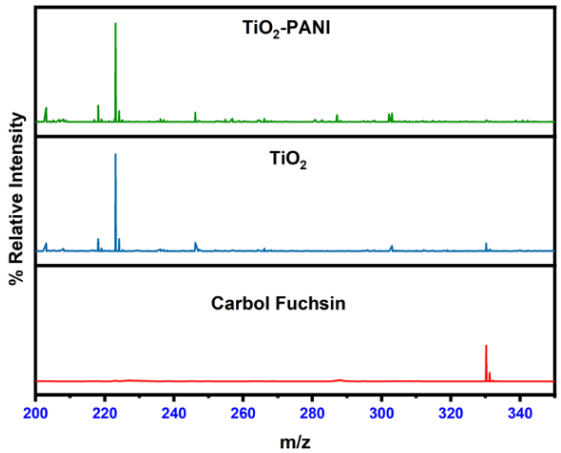

Fig. 19. Mass spectrum of the raw CF dye and treated dye solution

3.2.6. *Kinetic study*

The kinetic study is useful for in elucidating the order of a reaction and determining the half-life of a reaction. The order of the degradation reaction of CF dye is determined by Equation 4 [88].

$$\ln \frac{C_o}{C_t} = k_{app} t \quad (4)$$

where C_o represents the concentration of reactants at times 0 and C_t is the concentration of reactants at time t, k_{app} denotes the apparent pseudo-first-order rate constant of the reaction. The relationship between (C_o/C_t) and irradiation time (t) is graphically dependent in Figure 20.

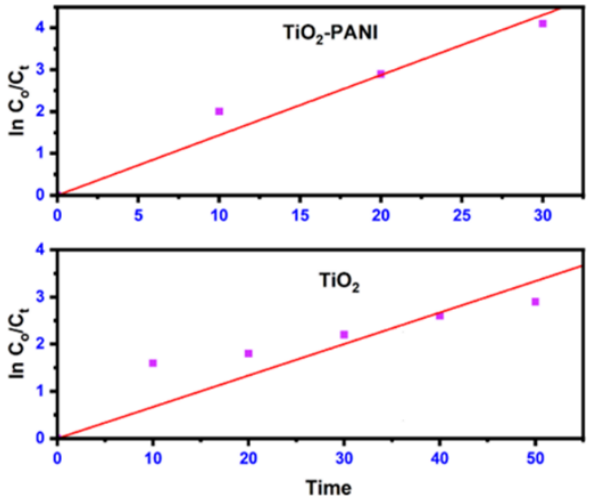

Fig. 20. Pseudo-first-order kinetics for the photocatalytic degradation of Carbol Fuchsin using TiO_2 and TiO_2-PANI nanocomposite

It can be seen from Figure 20, that the plot of ln (C_o/C_t) versus irradiation time (t) exhibits a linear relationship between them. The slope of this linear regression provides the apparent first-order rate constant for the degradation of the Carbol fuchsin dye.

The half-life for the CF dye degradation was determined using the following Equation 5,

$$t_{1/2} = \ln 2/ k = 0.6931 / k_{app} \quad (5)$$

The linear regression coefficient (R^2), pseudo-first-order rate constant and the half-life for the degradation of the CF dye are summarized in .

3.2.7. *Effect of Hydrogen peroxide in sunlight and reactor for degradation of CF dye*

The major role in the degradation of organic contaminants or dyes is played by reactive oxygen species (ROS) such as OH^-, O_2^- etc.

[DOI: 10.22068/ijmse.3511]

Table 4. Linear regression coefficient, apparent rate constant, and half-life of the degradation of CF dye using TiO_2 nanoparticles and TiO_2-PANI nanocomposites.

Name of the Catalyst	Linear regression coefficient (R^2)	Apparent rate constants (kapp) (min^{-1})	The half-life (min)
TiO_2	0.9834	0.0667	10.39
TiO_2-PANI	0.9606	0.1436	4.82

The results as presented in proves that the presence of PANI on the TiO_2 surface enhances the apparent rate constant and reduces the half-life in comparison to pure TiO_2.

These ROS in combination with valence electrons of metal oxide, combine with these species over the surface catalyst combines with dyes and degrade these dyes effectively.

Here we have conducted a small experiment to investigate the degradation pattern of CF dye in the presence and absence of hydrogen peroxide which is a ROS-generating species under mercury vapour reactor and conventional sunlight over the catalyst surface i.e. TiO_2 and TiO_2-PANI nanocomposite. The optimum conditions of CF dye and catalyst were kept constant such as 20 ppm CF dye, 8 g/L TiO_2, TiO_2-PANI catalyst concentration at neutral pH, and 20 ml of 30% H_2O_2 solution was mixed in this batch experiment process. Since, H_2O_2 is ROS generating species and hence it generates OH^-, O_2 in combination with electrons of the valence band and also alters the recombination of the (h^+/e^-) pair. Thus, after completion of this setup in the presence of sunlight and Hg- vapor reactor it was observed that the bare TiO_2 in combination with H_2O_2 in Hg vapor and sunlight degrades the CF dye in 50 minutes and 40 minutes respectively. While the TiO_2-PANI nanocomposite shows very rapid results for the same experimental conditions and degrades the CF dye in 35 and 30 minutes for TiO_2-PANI nanocomposite in Hg- vapor rector and sunlight respectively in the presence of H_2O_2 ROS generating species. Thus, the presence of ROS-generating species effectively degrades the 100% CF dye through the TiO_2 and TiO_2-PANI nanocomposite catalyst surface. The results of this experiment are summarized in Figure 21.

3.2.8. Detection of Reactive oxygen species (ROS) by Scavenging study

The advanced oxidation process (AOP) is strongly affected by the presence of reactive oxygen species like OH^-, O_2^-, O^{2-} etc. Thus, these ROS which effectively participate in the AOP can be studied with the help of scavenging study. In the present study common scavengers (ROS trappers) such as benzoquinone (BZQ), isopropyl alcohol (IPA), and ethylenediammine tetra acetic acid (EDTA) were used.

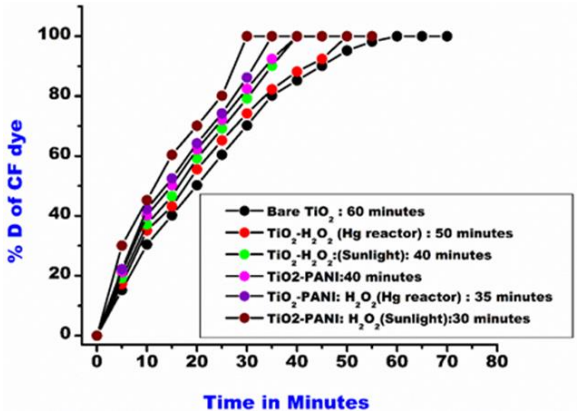

Fig. 21. Photocatalytic Degradation of CF dye using TiO_2 and TiO_2-PANI catalysed by hydrogen peroxide under sunlight and Hg-Vapour reactor

During the batch experiment process study of contact time when 5 mmole solution of IPA was added, it was observed that the photodegradation efficiency of CF dye through both the TiO_2-PANI catalyst was declined by the rate of approximately 9.5% in contrast to the solution of TiO_2-PANI catalyst which was not containing IPA scavenger. Whereas with the addition of benzoquinone and EDTA solutions with the same quantity of 5 mmole, the degradation efficiency declined at the rate of 28.52% and 31.45 % respectively. Thus in the overall experiment, EDTA was observed to be a more suitable scavenger for the photocatalytic degradation of CF dye. Moreover, the experiments also confirm the ROS OH^-, O_2^-, O^{2-} etc. which are most important in the AOP processes. This confirms that the generation of electrons through the valence band of TiO_2-PANI catalyst in combination with aqua molecules generates ROS which are highly effective in the photodegradation of organic molecules such as CF dye. The diagrammatic presentation of the scavenging study experiment for the TiO_2-PANI catalyst is as shown in Figure 22.

[DOI: 10.22068/ijmse.3511]

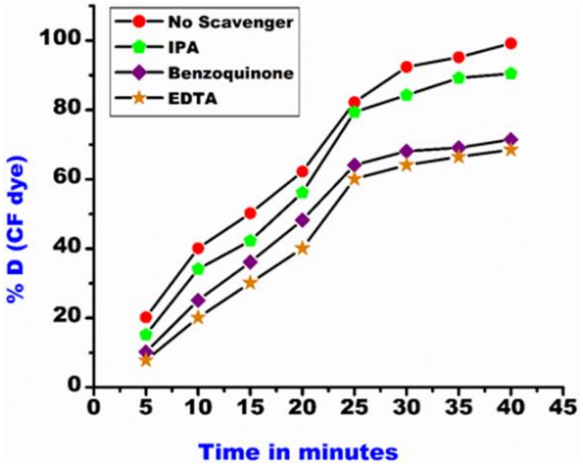

Fig. 22. Radical scavenging experiments for CF dye at TiO_2-PANI catalyst

3.2.9. Comparison of the efficiency of the prepared catalysts

As per existing literature, the TiO_2-PANI nanocomposite has been identified as more efficient. The application of these catalysts in pollutant degradation is shown Table 5. In the present study, the catalysts, namely the TiO_2-PANI nanocomposite are found to be more effective than pure TiO_2. Remarkably, the TiO_2-PANI nanocomposite achieved nearly complete degradation (almost 100%) of Carbol fuchsin (CF) dye within 40 minutes, surpassing the performance of the TiO_2, which required 60 minutes for the degradation of the same dye.

4. CONCLUSIONS

In the present study, the bare TiO_2 and TiO_2-PANI nanocomposites were prepared using sol-gel and chemical oxidative polymerization techniques, respectively. The UV analysis revealed that TiO_2 selectively absorbs UV light, while the TiO_2-PANI nanocomposite exhibits light absorption across both UV and visible regions. The band gap energy of bare TiO_2 and TiO_2-PANI nanocomposite were 3.32 eV and 2.88 eV respectively. The incorporation of PANI enhances visible light absorption, reduces the band gap energy, delays the electron-hole recombination, and thereby enhances the photocatalytic efficiency of the TiO_2-PANI nanocomposite.

The XRD results indicated the presence of a tetragonal phase of TiO_2 (anatase) in both TiO_2 and TiO_2-PANI nanocomposite, a finding validated by the Raman and TEM analysis. The average crystallite size was determined to be 13.87 nm for TiO_2 and 10.76 nm for the TiO_2-PANI nanocomposite. TGA results confirmed that the TiO_2-PANI has higher thermal stability compared to PANI, with TiO_2 exhibiting the highest thermal stability. TEM analysis revealed the distribution of lattice planes in two different directions, confirming the presence of the polycrystalline anatase TiO_2 in the SAED patterns. These patterns suggest many lattice planes that align well with the XRD observations.

The photocatalytic performance of both catalysts was evaluated against the Carbol Fuchsin dye. The TiO_2-PANI nanocomposite emerged as an exceptional photocatalyst, completely degrading Carbol Fuchsin dye within a remarkably short timeframe of 40 minutes, surpassing the performance of the pure TiO_2. The enhanced degradation efficiency of this catalyst was due to the presence of PANI. It contributes to increased light absorption in both UV and visible regions while simultaneously inhibiting electron-hole recombinations.

DECLARATION OF COMPETING INTEREST

The authors declare that they have no known competing financial interests or personal relationships that could have appeared to influence the work reported in this paper.

Table 5. Comparative study of TiO_2 and TiO_2-PANI nanocomposite against pollutant degradation

Catalyst	Dye	Degradation (%)	References
TiO_2	Methylene blue	34%	[87]
	Methylene blue	89.57%	[89]
	Reactive Black-5	10%	[90]
TiO_2-PANI nanocomposite	Methylene blue	80%	[87]
	Methylene blue	98.77%	[89]
	Reactive Black-5	96%	[90]
	Methyl orange and Orange II	94.2%	[91]

[DOI: 10.22068/ijmse.3511]

ACKNOWLEDGMENTS

The authors are grateful to acknowledge the Center for Materials for Electronic Technology(C-MET), Pune for the Raman and BET analysis; The Sophisticated Test and Instrumentation Center (STIC), Cochin University of Science and Technology Campus, Kochi, Kerala for the XRD, EDAX, SEM, TEM; University Institute of Chemical Technology, KBCNMU, Jalgaon for TGA and the H.P.T. Arts & R.Y.K. Science College, Nashik for UV analysis. The authors are grateful to the Loknete Vyankatrao Hiray Arts, Science, and Commerce College Panchavati, Nashik for providing research facilities.

RESEARCH HIGHLIGHTS

- A hybrid composite TiO_2-Polyaniline (PANI) nanocomposite was synthesized using the chemical oxidative polymerization method.
- The XRD analysis confirmed the presence of Anatase TiO_2. The average crystallite size of TiO_2 was 13.87 in pure form and 10.76 nm in the composite TiO_2-PANI.
- The TiO_2 exhibits absorption in the UV region, while its composite TiO_2-PANI nanocomposite absorbs across both UV and Visible regions.
- Robust degradation of Carbol Fuchsin dye was achieved within 40 minutes, indicating a promising photocatalytic activity.

REFERENCES

[1]. Muralikrishna, I. V.; Manickam, V. "Introduction. In Environmental Management"; 2017; 1–4.

[2]. Yadav, P.; Usha, K.; Singh, B. "Chapter 10-Air Pollution Mitigation and Global Dimming: A Challenge to Agriculture under Changing Climate". In Climate Change and Crop Stress; Shanker, A. K., Shanker, C., Anand, A., Maheswari, M., Eds.; Academic Press, 2022; 271–298.

[3]. Ukaogo, P. O.; Ewuzie, U.; Onwuka, C. V. "Environmental Pollution: Causes, Effects, and the Remedies"; INC, 2020.

[4]. Ingale, R. S.; Bhimrao Koli, P.; Shinde, S. G.; Khamkar, K. A.; Ahire, S. A.; Patil, I. J. "The Al^{3+} doped Modified ZnO Sensor Material: Fabrication, Characterization and Gas Sensing Characteristics of Some Environmental Pollutant and Greenhouse Gases". In Journal of Physics: Conference Series; 2023; Vol. 2426, 012050.

[5]. Ahire, S. A.; Koli, P. B.; Patil, A. V.; Jagdale, B. S.; Bachhav, A. A.; Pawar, T. B. "Designing of Screen-Printed Stannous Oxide (SnO_2) Thick Film Sensors Modified by Cobalt and Nitrogen Elements for Sensing Some Toxic Gases and Volatile Organic Compounds". Curr. Res. Green Sustain. Chem. 2021, 4, 100213.

[6]. Ameta, S. C. Chapter 1– "Introduction". Adv. Oxid. Process. Wastewater Treat. Emerg. Green Chem. Technol. 2018, 1–12.

[7]. Rathi, B. S.; Kumar, P. S.; Vo, D. V. N. "Critical Review on Hazardous Pollutants in Water Environment: Occurrence, Monitoring, Fate, Removal Technologies and Risk Assessment". Sci. Total Environ. 2021, 797, 149134.

[8]. Abu Shmeis, R. M. "Chapter Four-Nanotechnology in Wastewater Treatment. In Environmental Nanotechnology: Implications and Applications"; Turan, N. B., Engin, G. O., Bilgili, M. S., Eds.; Comprehensive Analytical Chemistry; Elsevier, 2022; Vol. 99, 105–134.

[9]. Maheshwari, K.; Agrawal, M.; Gupta, A. B. "Dye Pollution in Water and Wastewater. In Novel Materials for Dye-containing Wastewater Treatment". Muthu, S. S., Khadir, A., Eds.; Springer Singapore: Singapore, 2021; 1–25.

[10]. Rafiq, A.; Ikram, M.; Ali, S.; Niaz, F.; Khan, M.; Khan, Q.; Maqbool, M. "Photocatalytic Degradation of Dyes Using Semiconductor Photocatalysts to Clean Industrial Water Pollution". J. Ind. Eng. Chem. 2021, 97, 111–128.

[11]. Kumar, A. "A Review on the Factors Affecting the Photocatalytic Degradation of Hazardous Materials". Mater. Sci. Eng. Int. J. 2017, 1 (3), 106–114.

[12]. Castillo-Suárez, L. A.; Sierra-Sánchez, A. G.; Linares-Hernández, I.; Martínez-Miranda, V.; Teutli-Sequeira, E. A. "A Critical Review of Textile Industry Wastewater: Green Technologies for the Removal of Indigo Dyes". Int. J. Environ. Sci. Technol. 2023, 20 (9), 10553–10590.

[13]. Lellis, B.; Fávaro-Polonio, C. Z.;

[DOI: 10.22068/ijmse.3511]

Pamphile, J. A.; Polonio, J. C. “Effects of Textile Dyes on Health and the Environment and Bioremediation Potential of Living Organisms”. Biotechnol. Res. Innov. 2019, 3 (2), 275–290.

[14]. Chung, K.-T. “Azo Dyes and Human Health: A Review”. J. Environ. Sci. Heal. Part C, Environ. Carcinog. Ecotoxicol. Rev. 2016, 34 (4), 233–261.

[15]. Roy, M.; Saha, R. “6- Dyes and Their Removal Technologies from Wastewater: A Critical Review”. In Intelligent Environmental Data Monitoring for Pollution Management; Bhattacharyya, S., Mondal, N. K., Platos, J., Snášel, V., Krömer, P., Eds.; Intelligent Data-Centric Systems; Academic Press, 2021; 127–160.

[16]. Dadashi, J.; Ali Ghasemzadeh, M.; Alipour, S.; Zamani, F. “A Review on Catalytic Reduction/Degradation of Organic Pollution through Silver-Based Hydrogels”. Arab. J. Chem. 2022, 15 (9), 104023.

[17]. Rathi, B. S.; Kumar, P. S. “Application of Adsorption Process for Effective Removal of Emerging Contaminants from Water and Wastewater”. Environ. Pollut. 2021, 280, 116995.

[18]. Fawzi Suleiman Khasawneh, O.; Palaniandy, P. “Removal of Organic Pollutants from Water by Fe_2O_3/TiO_2 Based Photocatalytic Degradation: A Review”. Environ. Technol. Innov. 2021, 21, 101230.

[19]. Koli, P. B.; Birari, M. D.; Ahire, S. A.; Shinde, S. G.; Ingale, R. S.; Patil, I. J. “Ferroso-Ferric Oxide (Fe_3O_4) Embedded g-C_3N_4 Nanocomposite Sensor Fabricated by Photolithographic Technique for Environmental Pollutant Gas Sensing and Relative Humidity Characteristics”. Inorg. Chem. Commun. 2022, 146, 110083.

[20]. Islam, M.; Kumar, S.; Saxena, N.; Nafees, A. “Photocatalytic Degradation of Dyes Present in Industrial Effluents: A Review”. ChemistrySelect 2023, 8 (26), e202301048.

[21]. Ferreira, V. R. A.; Santos, P. R. M.; Silva, C. I. Q.; Azenha, M. A. “Latest Developments on TiO_2-Based Photocatalysis: A Special Focus on Selectivity and Hollowness for Enhanced Photonic Efficiency”. Appl. Catal. A Gen. 2021, 623 (May), 118243.

[22]. Anucha, C. B.; Altin, I.; Bacaksiz, E.; Stathopoulos, V. N. “Titanium Dioxide (TiO_2)-Based Photocatalyst Materials Activity Enhancement for Contaminants of Emerging Concern (CECs) Degradation: In the Light of Modification Strategies”. Chem. Eng. J. Adv. 2022, 10 (September 2021), 100262.

[23]. Satish A. Ahire, Ashwini A. Bachhav, Vinayak R. Bagul, Bajirao B. Ahire, U. J. T. A “Literature Review on Synthesis Approaches of Metal Doped Titanium Dioxide”. Int. J. Emerg. Technol. Innov. Res. 2019, 6 (2).

[24]. Reghunath, S.; Pinheiro, D.; KR, S. D. “A Review of Hierarchical Nanostructures of TiO_2: Advances and Applications”. Appl. Surf. Sci. Adv. 2021, 3 (January), 100063.

[25]. Bardin, V. A.; Vorotnikov, Y. A.; Asanov, I. P.; Vorotnikova, N. A.; Shestopalov, M. A. “Visible-Light Active S-Scheme Heterojunction Photocatalyst Based on Nanosized Anatase TiO_2 and Octahedral Iodide Molybdenum Clusters”. Appl. Surf. Sci. 2023, 612, 155738.

[26]. Xiaodan Chen, S. N. H. and M. A. va. H. “Heating-Induced Transformation of Anatase TiO_2 Nanorods into Rock-Salt TiO Nanoparticles: Implications for Photocatalytic and Gas Sensing Applications”. ACS Appl.Nano Mater. 2022, 5, 1600–1606.

[27]. Luttrell, T.; Halpegamage, S.; Tao, J.; Kramer, A.; Sutter, E.; Batzill, M. “Why Is Anatase a Better Photocatalyst than Rutile? -Model Studies on Epitaxial TiO_2 Films”. Sci. Rep. 2015, 4, 4043.

[28]. Athanasekou, C. P.; Likodimos, V.; Falaras, P. “Recent Developments of TiO_2 Photocatalysis Involving Advanced Oxidation and Reduction Reactions in Water”. J. Environ. Chem. Eng. 2018, 6 (6), 7386–7394.

[29]. Motamedisade, A.; Heydari, A.; Osborn, D. J.; Alotabi, A. S.; Andersson, G. G. “Au_9 Clusters Deposited as Co-Catalysts on S-Modified Mesoporous TiO_2 for Photocatalytic Degradation of Methyl Orange”. Appl. Surf. Sci. 2024, 655, 159475.

[DOI: 10.22068/ijmse.3511]

[30]. Kamat, P. V. "Photochemistry on Nonreactive and Reactive (Semiconductor) Surfaces". Chem. Rev. 1993, 93 (1), 267–300.
[31]. Lee, Y. J.; Lee, H. S.; Lee, C. G.; Park, S. J.; Lee, J.; Jung, S.; Shin, G. A. "Application of PANI/TiO_2 Composite for Photocatalytic Degradation of Contaminants from Aqueous Solution". Appl. Sci. 2020, 10 (19), 2–13.
[32]. Khor, S.-H.; Lee, M. L.-Y.; Phang, S.-W.; Basirun, W. J.; Juan, J.-C. "Effect of Morphology on the Electrical Conductivity of Polyaniline as Potential Photocatalyst". Polym. Sci. Ser. B 2023, 65 (6), 873–880.
[33]. Olad, A.; Behboudi, S.; Entezami, A. A. "Preparation, Characterization and Photocatalytic Activity of TiO_2/Polyaniline Core-Shell Nanocomposite". Bull. Mater. Sci. 2012, 35 (5), 801–809.
[34]. Zhu, Y.; Xu, S.; Yi, D. "Photocatalytic Degradation of Methyl Orange Using Polythiophene/Titanium Dioxide Composites". React. Funct. Polym. 2010, 70 (5), 282–287.
[35]. Xueyan Li, Desong Wang, Qingzhi Luo, Jing An, Yanhong Wang, G. C. "Surface Modification of Titanium Dioxide Nanoparticles by Polyaniline via an in Situ Method". J. Chem. Technol. Biotechnol. 2008, 1558–1564.
[36]. Rahman, K. H.; Kar, A. K. "Titanium-Di-Oxide (TiO_2) Concentration-Dependent Optical and Morphological Properties of PAni-TiO_2 Nanocomposite". Mater. Sci. Semicond. Process. 2020, 105 (September 2019), 104745.
[37]. Yang, H.; Dai, K.; Zhang, J.; Dawson, G. "Inorganic-Organic Hybrid Photocatalysts: Syntheses, Mechanisms, and Applications". Chinese J. Catal. 2022, 43 (8), 2111–2140.
[38]. Kumar, A.; Raorane, C. J.; Syed, A.; Bahkali, A. H.; Elgorban, A. M.; Raj, V.; Kim, S. C. "Synthesis of TiO_2, TiO_2/PAni, TiO_2/PAni/GO Nanocomposites and Photodegradation of Anionic Dyes Rose Bengal and Thymol Blue in Visible Light". Environ. Res. 2023, 216, 114741.
[39]. Patil, M. R.; Khairnar, S. D.; Shrivastava, V. S. "Synthesis, Characterisation of Polyaniline–Fe_3O_4 Magnetic Nanocomposite and Its Application for Removal of an Acid Violet 19 Dye". Appl. Nanosci. 2016, 6 (4), 495–502.
[40]. Koli, P. B.; Kapadnis, K. H.; Deshpande, U. G.; Patil, M. R. "Fabrication and Characterization of Pure and Modified Co_3O_4 Nanocatalyst and Their Application for Photocatalytic Degradation of Eosine Blue Dye: A Comparative Study". J. Nanostructure Chem. 2018, 8 (4), 453–463.
[41]. Gilja, V.; Novaković, K.; Travas-Sejdic, J.; Hrnjak-Murgić, Z.; Roković, M. K.; Žic, M. "Stability and Synergistic Effect of Polyaniline/TiO_2 Photocatalysts in Degradation of Azo Dye in Wastewater". Nanomaterials 2017, 7 (12).
[42]. Yang, C.; Dong, W.; Cui, G.; Zhao, Y.; Shi, X.; Xia, X.; Tang, B.; Wang, W. "Enhanced Photocatalytic Activity of PANI/TiO_2 Due to Their Photosensitization-Synergetic Effect". Electrochim. Acta 2017, 247, 486–495.
[43]. Ahire, S. A.; Bachhav, A. A.; Jagdale, B. S.; Patil, A. V.; Koli, P. B.; Pawar, T. B. "Amalgamation of ZrO_2-PANI Nanocomposite Polymeric Material: Characterization and Expeditious Photocatalytic Performance Towards Carbol Fuchsin (CF) Dye and Kinetic Study". J. Inorg. Organomet. Polym. Mater. 2023, 33, 1357–1368.
[44]. Yang, H.; Zhang, K.; Shi, R.; Li, X.; Dong, X.; Yu, Y. "Sol-Gel Synthesis of TiO_2 Nanoparticles and Photocatalytic Degradation of Methyl Orange in Aqueous TiO_2 Suspensions". J. Alloys Compd. 2006, 413 (1–2), 302–306.
[45]. Mugundan, S.; Rajamannan, B.; Viruthagiri, G.; Shanmugam, N.; Gobi, R.; Praveen, P. "Synthesis and Characterization of Undoped and Cobalt-Doped TiO_2 Nanoparticles via Sol–Gel Technique". Appl. Nanosci. 2015, 5 (4), 449–456.
[46]. Deivanayaki, S.; Ponnuswamy, V.; Ashokan, S.; Jayamurugan, P.; Mariappan, R. "Synthesis and Characterization of TiO_2-Doped Polyaniline Nanocomposites by Chemical Oxidation Method". Mater. Sci. Semicond. Process. 2013, 16 (2), 554–559.

[DOI: 10.22068/ijmse.3511]

[47]. Faraji, M.; Yamini, Y.; Salehi, N. "3- Characterization of Magnetic Nanomaterials". Ahmadi, M., Afkhami, A., Madrakian, T. B. T.-M. N. in A. C., Eds.; Elsevier, 2021; 39–60.
[48]. Wang, J.; Ni, X. "Photoresponsive Polypyrrole- TiO_2 Nanoparticles Film Fabricated by a Novel Surface Initiated Polymerization". Solid State Commun. 2008, 146 (5), 239–244.
[49]. Li, X.; Wang, D.; Cheng, G.; Luo, Q.; An, J.; Wang, Y. "Preparation of Polyaniline-Modified TiO_2 Nanoparticles and Their Photocatalytic Activity under Visible Light Illumination". Appl. Catal. B Environ. 2008, 81 (3), 267–273.
[50]. Zhang, H.; Zong, R.; Zhao, J.; Zhu, Y. Dramatic, "Visible Photocatalytic Degradation Performances Due to Synergetic Effect of TiO_2 with PANI". Environ. Sci. Technol. 2008, 42 (10), 3803–3807.
[51]. Neppolian, B.; Wang, Q.; Yamashita, H.; Choi, H. "Synthesis and Characterization of ZrO_2-TiO_2 Binary Oxide Semiconductor Nanoparticles: Application and Interparticle Electron Transfer Process". Appl. Catal. A Gen. 2007, 333 (2), 264–271.
[52]. Xiong, S.; Wang, Q.; Xia, H. "Template Synthesis of Polyaniline/TiO_2 Bilayer Microtubes". Synth. Met. 2004, 146 (1), 37–42.
[53]. Tauc, J.; Grigorovici, R.; Vancu, A. "Optical Properties and Electronic Structure of Amorphous Germanium". Phys. status solidi 1966, 15 (2), 627–637.
[54]. Makuła, P.; Pacia, M.; Macyk, W. "How To Correctly Determine the Band Gap Energy of Modified Semiconductor Photocatalysts Based on UV–Vis Spectra". J. Phys. Chem. Lett. 2018, 9 (23), 6814–6817.
[55]. Dette, C.; Pérez-Osorio, M. A.; Kley, C. S.; Punke, P.; Patrick, C. E.; Jacobson, P.; Giustino, F.; Jung, S. J.; Kern, K. "TiO_2 Anatase with a Bandgap in the Visible Region". Nano Lett. 2014, 14 (11), 6533–6538.
[56]. Abdi, J.; Yahyanezhad, M.; Sakhaie, S.; Vossoughi, M.; Alemzadeh, I. "Synthesis of Porous TiO_2/ZrO_2 Photocatalyst Derived from Zirconium Metal Organic Framework for Degradation of Organic Pollutants under Visible Light Irradiation". J. Environ. Chem. Eng. 2019, 7 (3), 103096.
[57]. Raveendran, L.; Veerapandy, V.; Mohan, B.; Balakrishnan, K.; Selvarajan, P. "Effect of Morphology on the Photocatalytic Property of PANI/TiO_2 on Some Synthetic Dyes". Mater. Res. Express 2019, 6 (12), 125040.
[58]. Li, J.; Sun, J. "Application of X-Ray Diffraction and Electron Crystallography for Solving Complex Structure Problems". Acc. Chem. Res. 2017, 50 (11), 2737–2745.
[59]. Gao, L.; Yin, C.; Luo, Y.; Duan, G. "Facile Synthesis of the Composites of Polyaniline and TiO_2 Nanoparticles Using Self-Assembly Method and Their Application in Gas Sensing". Nanomaterials 2019, 9 (4).
[60]. Momma, K.; Izumi, F. "VESTA 3 for Three-Dimensional Visualization of Crystal, Volumetric and Morphology Data". J. Appl. Crystallogr. 2011, 44 (6), 1272–1276.
[61]. Vadiraj, K. T.; Belagali, S. "Characterization of Polyaniline for Optical and Electrical Properties". IOSR J. Appl. Chem 2015, 8 (1), 53–56.
[62]. Mahajan, A. P.; Kondawar, S. B.; Mahore, R. P.; Meshram, B. H.; Virutkar, P. D. "Polyaniline/MnO_2 Nanocomposites Based Stainless Steel Electrode Modified Enzymatic Urease Biosensor". Procedia Mater. Sci. 2015, 10, 699–705.
[63]. Hashemi Monfared, A.; Jamshidi, M. "Synthesis of Polyaniline/Titanium Dioxide Nanocomposite (PAni/TiO_2) and Its Application as Photocatalyst in Acrylic Pseudo Paint for Benzene Removal under UV/VIS Lights". Prog. Org. Coatings 2019, 136 (March 2018), 105257.
[64]. Ambalagi, S. M.; Devendrappa, M.; Nagaraja, S.; Sannakki, B. "Dielectric Properties of PANI/CuO Nanocomposites". IOP Conf. Ser. Mater. Sci. Eng. 2018, 310 (1), 12081.
[65]. Raval, N.; Maheshwari, R.; Kalyane, D.; Youngren-Ortiz, S. R.; Chougule, M. B.; Tekade, R. K. "Importance of Physicochemical Characterization of Nanoparticles in Pharmaceutical Product Development"; Elsevier Inc., 2018.

[DOI: 10.22068/ijmse.3511]

[66]. Akhtar, K.; Khan, S. A.; Khan, S. B.; Asiri, A. M. "Scanning Electron Microscopy: Principle and Applications in Nanomaterials Characterization". 2018.
[67]. Sun, C.; Lux, S.; Müller, E.; Meffert, M.; Gerthsen, D. "Versatile Application of a Modern Scanning Electron Microscope for Materials Characterization". J. Mater. Sci. 2020, 55 (28), 13824–13835.
[68]. Sambaza, S. S.; Maity, A.; Pillay, K. "Polyaniline-Coated TiO_2 Nanorods for Photocatalytic Degradation of Bisphenol A in Water". ACS Omega 2020, 5 (46), 29642–29656.
[69]. Li, C.; Zhou, T.; Zhu, T.; Li, X. "Enhanced Visible Light Photocatalytic Activity of Polyaniline–Crystalline TiO_2–Halloysite Composite Nanotubes by Tuning the Acid Dopant in the Preparation". RSC Adv. 2015, 5 (119), 98482–98491.
[70]. Zhang, H.; Zong, R.; Zhu, Y. "Photocorrosion Inhibition and Photoactivity Enhancement for Zinc Oxide via Hybridization with Monolayer Polyaniline". J. Phys. Chem. C 2009, 113 (11), 4605–4611.
[71]. Tran, V. Van; Nu, T. T. V.; Jung, H. R.; Chang, M. "Advanced Photocatalysts Based on Conducting Polymer/Metal Oxide Composites for Environmental Applications". Polymers (Basel). 2021, 13 (18).
[72]. Bergström, J. "Experimental Characterization Techniques". 2015.
[73]. Cong, X.; Liu, X.-L.; Lin, M.-L.; Tan, P.-H. "Application of Raman Spectroscopy to Probe Fundamental Properties of Two-Dimensional Materials". npj 2D Mater. Appl. 2020, 4 (1), 13.
[74]. Raman, C. V.; Krishnan, K. S. "A New Type of Secondary Radiation". Nature 1928, 121 (3048), 501–502.
[75]. El-Deen, S. S., A. M. Hashem, A. E. Abdel Ghany, S. Indris, H. Ehrenberg, A. M. & C. M. J. "Anatase TiO_2 Nanoparticles for Lithium-Ion Batteries". Ionics (Kiel). 2018, 24, 2925–2934.
[76]. Lv, H.; Wang, Y.; Pan, L.; Zhang, L.; Zhang, H.; Shang, L.; Qu, H.; Li, N.; Zhao, J.; Li, Y. "Patterned Polyaniline Encapsulated in Titania Nanotubes for Electrochromism". Phys. Chem. Chem. Phys. 2018, 20 (8), 5818–5826.
[77]. Zhang, L.; Wan, M. "Polyaniline/TiO_2 Composite Nanotubes". J. Phys. Chem. B 2003, 107 (28), 6748–6753.
[78]. Quillard, S.; Louarn, G.; Lefrant, S.; Macdiarmid, A. G. "Vibrational Analysis of Polyaniline: A Comparative Study of Leucoemeraldine, Emeraldine, and Pernigraniline Bases". Phys. Rev. B 1994, 50 (17), 12496–12508.
[79]. Rajisha, K. R.; Deepa, B.; Pothan, L. A.; Thomas, S. "Thermomechanical and Spectroscopic Characterization of Natural Fibre Composites". In Woodhead Publishing Series in Composites Science and Engineering; Zafeiropoulos, N. E. B. T.-I. E. of N. F. C. for M. P., Ed.; Woodhead Publishing, 2011; 241–274.
[80]. Pang, Y. L.; Lim, S.; Lee, R. K. L. "Enhancement of Sonocatalytic Degradation of Organic Dye by Using Titanium Dioxide (TiO_2)/Activated Carbon (AC) Derived from Oil Palm Empty Fruit Bunch". Environ. Sci. Pollut. Res. 2020, 27 (28), 34638–34652.
[81]. Mast, J.; Verleysen, E.; Hodoroaba, V. D.; Kaegi, R. "Characterization of Nanomaterials by Transmission Electron Microscopy: Measurement Procedures". Elsevier Inc., 2019.
[82]. Parveen, N.; Ansari, M. O.; Han, T. H.; Cho, M. H. "Simple and Rapid Synthesis of Ternary Polyaniline/Titanium Oxide/Graphene by Simultaneous TiO_2 Generation and Aniline Oxidation as Hybrid Materials for Supercapacitor Applications". J. Solid State Electrochem. 2017, 21 (1), 57–68.
[83]. Hidalgo, D.; Bocchini, S.; Fontana, M.; Saracco, G.; Hernández, S. "Green and Low-Cost Synthesis of PANI-TiO_2 Nanocomposite Mesoporous Films for Photoelectrochemical Water Splitting". RSC Adv. 2015, 5 (61), 49429–49438.
[84]. Bargui, M.; Messaoud, M.; Elleuch, K. "Electrophoretic Impregnation of Porous Anodizing Layer by Synthesized TiO_2 Nanoparticles". Surf. Eng. Appl. Electrochem. 2017, 53 (5), 467–474.
[85]. Zhang, D.; Lv, S.; Luo, Z. "A Study on the Photocatalytic Degradation Performance of a $[KNbO_3]0.9$-$[BaNi_{0.5}Nb_{0.5}O_{3-\delta}]_{0.1}$

[DOI: 10.22068/ijmse.3511]

Perovskite". RSC Adv. 2020, 10 (3), 1275–1280.

[86]. Zhang, D.; Lv, S.; Luo, Z. "A Study on the Photocatalytic Degradation Performance of a $[KNbO_3]_{0.9}$-$[BaNi_{0.5}Nb_{0.5}O_{3-\delta}]_{0.1}$ Perovskite". RSC Adv. 2020, 10 (3), 1275–1280.

[87]. Mahmoodi, N. M. "Binary Catalyst System Dye Degradation Using Photocatalysis". Fibers Polym. 2014, 15 (2), 273–280.

[88]. Wang, F.; Min, S. X. "TiO_2/Polyaniline Composites: An Efficient Photocatalyst for the Degradation of Methylene Blue under Natural Light". Chinese Chem. Lett. 2007, 18 (10), 1273–1277.

[89]. Azeez, F.; Al-Hetlani, E.; Arafa, M.; Abdelmonem, Y.; Nazeer, A. A.; Amin, M. O.; Madkour, M. "The Effect of Surface Charge on Photocatalytic Degradation of Methylene Blue Dye Using Chargeable Titania Nanoparticles". Sci. Rep. 2018, 8 (1), 1–9.

[90]. Kaur, H.; Kumar, S.; Kaushal, S.; Badru, R.; Singh, P. P.; Singh, J.; Singh, K.; Pugazhendhi, A. "Highly Customized Porous TiO_2-PANI Nanoparticles with Excellent Photocatalytic Efficiency for Dye Degradation". Environ. Res. 2022, 114960.

[91]. Jumat, N. A.; Wai, P. S.; Ching, J. J.; Basirun, W. J. "Synthesis of Polyaniline-TiO_2 Nanocomposites and Their Application in Photocatalytic Degradation". Polym. Polym. Compos. 2017, 25 (7), 507–514.

[92]. Cheng, Y.; An, L.; Zhao, Z.; Wang, G. "Preparation of Polyaniline/ TiO_2 Composite Nanotubes for Photodegradation of AZO Dyes". J. Wuhan Univ. Technol. Sci. Ed. 2014, 29 (3), 468–472.

[DOI: 10.22068/ijmse.3511]